Available online at www.sciencedirect.com
ScienceDirect
Journal of Power Sources 171 (2007) 601–609
JOURNAL OF POWER SOURCES
www.elsevier.com/locate/jpowsour

# 3D modeling of anode-supported planar SOFC with internal reforming of methane

Kasra Nikooyeh, Ayodeji A. Jeje, Josephine M. Hill *

*Department of Chemical and Petroleum Engineering, University of Calgary, 2500 University Dr NW, Calgary, Alberta T2N 1N4, Canada*

Received 30 May 2007; received in revised form 27 June 2007; accepted 3 July 2007
Available online 10 July 2007

**Abstract**

Deposition of carbon on conventional anode catalysts and formation of large temperature gradients along the cell are the main barriers for implementing internal reforming in solid oxide fuel cell (SOFC) systems. Mathematical modeling is an essential tool to evaluate the effectiveness of the strategies to overcome these problems. In the present work, a three-dimensional model for a planar internal reforming SOFC is developed. A co-flow system with no pre-reforming, methane fuel utilization of 75%, voltage of 0.7 V and current density of 0.65 A $cm^{-2}$ was used as the base case. The distributions of both temperature and gas composition through the gas channels and PEN (positive electrode/electrolyte/negative electrode) structure were studied using the developed model. The results identified the most susceptible areas for carbon formation and thermal stress according to the methane to steam ratio and temperature gradients, respectively. The effects of changing the inlet gas composition through recycling were also investigated. Recycling of the anode exhaust gas, at an optimum level of 60% for the conditions studied, has the potential to significantly decrease the temperature gradients and reduce the carbon formation at the anode, while maintaining a high current density.


*Keywords:* SOFC; Direct internal reforming; Methane; Anode-supported; Recycling

## 1. Introduction

Solid oxide fuel cells (SOFC) have attracted considerable interest during the past decade as highly effective sources of electrical energy [1]. This type of fuel cell operates at relatively high temperatures (650–950 °C) with hydrocarbons or hydrogen as the fuel at the anode and air as the oxidant at the cathode. Internal reforming of methane within an SOFC to produce hydrogen in situ can maximize the efficiency and simplicity of the process by combining the reforming and electrochemical processes. The two main drawbacks to internal reforming are the large temperature gradients generated within the fuel cell and the deposition of carbon on the anode that leads to deactivation of the electrocatalysts.

Steam reforming is a highly endothermic reaction, whereas electrochemical oxidation is an exothermic reaction [2–5]. At the inlet of a cell where the fuel, typically methane, concentration is high, the reforming rate dominates such that the inlet region cools below the feed temperature. As the fuel flows into the cell the relative amount of hydrogen to methane increases and the electrochemical reaction eventually dominates resulting in a temperature increase downstream in the cell. The steep temperature gradients that result from the localized heating and cooling within the cell can lead to significant thermal stresses in the solid structure and potentially to a system failure from crack formation in the cell.

The second drawback of steam reforming on conventional nickel/yttria-stabilized zirconia (Ni/YSZ) anodes is the tendency of Ni to catalyze carbon formation [6]. Eventual deactivation of the catalyst occurs if the rate of carbon deposition, occurring through reaction (1), exceeds the rate of its removal, occurring through reactions (2) and (3) [7–10]:

$$CH_4 \rightarrow C + 2H_2 \quad (1)$$

$$C + H_2O \rightarrow CO + H_2 \quad (2)$$

$$C + O^{2-} \rightarrow CO + 2e^- \quad (3)$$

* Corresponding author. Tel.: +1 403 210 9488; fax: +1 403 284 4852.
*E-mail address:* jhill@ucalgary.ca (J.M. Hill).

0378-7753/$ – see front matter © 2007 Elsevier B.V. All rights reserved.
doi:10.1016/j.jpowsour.2007.07.003

**Nomenclature**

| | |
|---|---|
| $A$ | area |
| $C_p$ | heat capacity at constant pressure |
| $D$ | diffusion coefficient |
| $D_h$ | hydraulic diameter |
| $E$ | energy |
| $E^0$ | reference reaction potential |
| $E_{OCV}$ | open circuit potential |
| $F$ | Faraday no. |
| $G$ | heat transfer parameter |
| $h$ | convective heat transfer coefficient |
| $H$ | height |
| $i$ | current density |
| $i_0$ | exchange current density |
| $k$ | conductive heat transfer coefficient |
| $L$ | cell length |
| $n_e$ | no. of electrons transferred in the reaction |
| $N$ | no. of moles |
| $N_i$ | molar flux of species $i$ |
| Nu | Nusselt no. |
| $P$ | pressure |
| Prandtl | Prandtl no. |
| $R$ | universal gas constant |
| $R_{5,6,7}$ | reaction rate (mol m$^{-2}$ s$^{-1}$) |
| Re | Reynolds no. |
| $t$ | thickness |
| $T$ | temperature |
| $u$ | linear velocity |
| $w$ | width |
| $X$ | mole fraction |
| $Z$ | distance in $z$-direction |

*Greek letters*

| | |
|---|---|
| $\gamma$ | heat transfer parameter |
| $\eta$ | potential (voltage) drop |
| $\nu_{ij}$ | stoichiometric coefficient |

*Subscripts*

| | |
|---|---|
| a | anode |
| act | activation |
| air | air |
| c | cathode |
| cb | catalyst bed |
| conc | concentration |
| e | electrolyte |
| f | fuel |
| fc | fuel channel |
| ic | interconnect |
| s | solid |
| t | total |

*Superscripts*

| | |
|---|---|
| Eff | effective |
| Ref | reference |
| TPB | triple phase boundary |

At lower temperatures – typically below 973 K – disproportionation of carbon monoxide (the so-called Boudouard reaction) can also serve as a carbon forming reaction as will be discussed later.

The rate of carbon formation is affected by the steam to hydrocarbon or carbon ratio [8,11,12], the current density [9,13,14], and the hydrogen to hydrocarbon ratio [15]. Higher steam to carbon ratios and higher current densities decrease the rate of carbon formation by enhancing removal of carbon from the surface through reactions (2) and (3) [9,13]. Higher current densities result in more oxygen anions diffusing through the electrolyte to the anode structure and production of more steam within the pores of the anode through the electrochemical reaction. Diffusion of oxygen anions is limited to the active region of the anode [16] and will not reduce carbon formation at the electrochemically inactive regions of thicker anodes in anode-supported systems. A higher ratio of hydrogen to methane will also decrease the rate of carbon formation by promoting the reverse of reaction (1) [17,18].

A promising way to resolve the problems of both carbon formation and steep temperature gradients in SOFC is to recycle part of the outlet stream from the anode [19–21]. This exhaust stream contains hydrogen ($H_2$, ~15%), water and a relatively high carbon dioxide ($CO_2$) to carbon monoxide (CO) ratio. Recycling of the outlet anode stream adjusts the inlet feed composition. Specifically, the concentration of methane ($CH_4$) is decreased and the concentrations of $H_2$ and $CO_2$ are increased. These changes result in a higher current density at the inlet, lower rate of carbon formation [2], and decreased steam make-up requirement [19]. In addition, temperature gradients in the cell are reduced because of the increase in the relative rate of the electrochemical reaction (reaction (3)) versus the rate of the reforming reaction (reaction (5), below). The amount of carbon formation is reduced from the higher concentrations of both hydrogen and carbon dioxide in the feed. Hydrogen impedes reaction (1), while carbon dioxide ($CO_2$) promotes the reverse Boudouard reaction [22,23] as shown in reaction (4):

$$CO_2 + C \rightarrow 2CO \quad (4)$$

In order to better understand the operation of SOFC, a number of theoretical models have been developed. Some studies have modeled various SOFC geometries for electrode- [1,24] and anode-supported [25–27] cells with either internal [25,26] or external reforming [27]. The results of these studies indicate the formation of large temperature gradients along the length of the cell when internal reforming is employed. The models published thus far, however, contain deficiencies such as modeling in only one or two dimensions rather than in three dimensions, assuming reactions occurring in the gas-phase are representative of the solid-phase reactions, and neglecting the effect of diffusion of gases through the PEN (positive electrode/electrolyte/negative electrode) structure in all directions. These deficiencies affect the reliability of the results and limit their usefulness.

In this study, we have developed a rigorous model of an SOFC with direct internal reforming in order to investigate the problems of carbon formation and temperature gradients within a cell

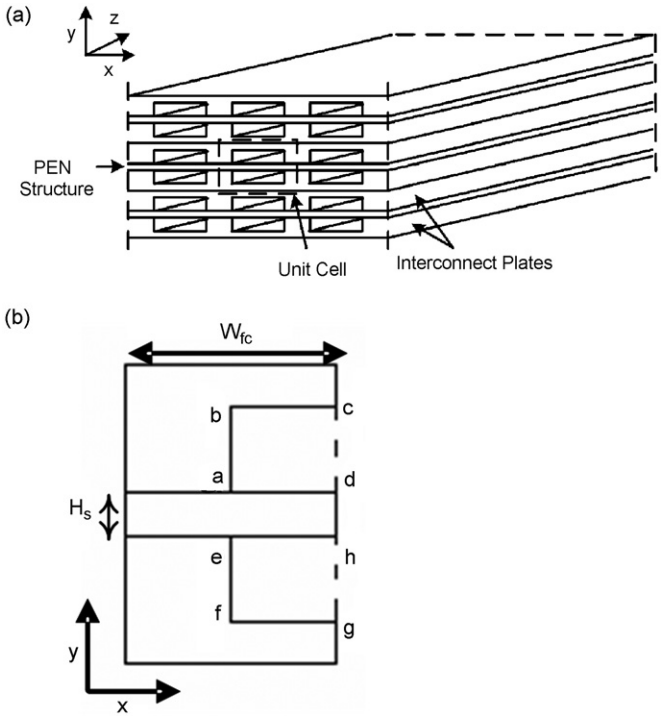


Fig. 1. Schematic of modeled system: (a) 3D view of three cells in a stack and (b) front view of half of one unit cell. The letters in (b) are those referred to in the boundary conditions in Table 2.

and stack. The three-dimensional model includes electrochemical reactions, and heat and mass transfer between the solid and gas phases, and is solved using COMSOL Multiphysics 3.2. The composition of the feed gas mixture, in particular the concentrations of $H_2$, $CH_4$, $H_2O$ and $CO_2$, is the main parameter varied in this study. Our results demonstrate that recycling of the anode exhaust gases is indeed a promising technique for regulating the temperature gradients and carbon formation within the cell.

## 2. System and model development

A three-dimensional mass and heat transfer model was developed for an anode-supported cell of planar geometry, as shown in Fig. 1. The PEN structure is between interconnects that form channels for air and fuel flow. In the model, the air and fuel flow co-currently over opposite sides of the PEN structure. The choice of co-current flow is discussed in Section 3. Calculations were performed on one unit cell in the stack. It will be shown that one unit cell is representative of the behavior of the entire stack, except at the edges of the stack where the boundary conditions may be different. As shown in Fig. 1a, there is a plane of symmetry in the centre of each unit cell and so the calculations required can be further reduced. In the presented results, the $x$, $y$ and $z$ dimensions have been normalized between 0 and 1, unless otherwise noted. A summary of system specifications is presented in Table 1.

Table 1
System specifications

| | |
|---|---|
| Gas inlet temperature | 1073 K |
| Current density ($i$) | 0.65 A cm$^{-2}$ |
| Air to fuel ratio | 8 |
| Anode thickness ($t_a$) | 1000 μm |
| Cathode thickness ($t_c$) | 50 μm |
| Flow arrangement | Co-current flow |
| Operating voltage | 0.7 V |
| Cell dimensions | 10 cm × 10 cm |
| Fuel utilization | 75% |
| Electrolyte thickness ($t_e$) | 10 μm |
| Channel dimensions ($w_{fc}$ × $H_{fc}$) | 5 cm × 2 cm |
| Steam to carbon ratio in fuel | 2 |

### 2.1. Mass balances

The following three surface reactions were considered in the model:

$$CH_4 + H_2O \overset{\text{reversible}}{\longleftrightarrow} CO + 3H_2 \quad (5)$$

$$CO + H_2O \overset{\text{reversible}}{\longleftrightarrow} CO_2 + H_2 \quad (6)$$

$$H_2 + O^{2-} \rightarrow H_2O + 2e^- \quad (7)$$

The steam reforming and water-gas shift reactions (5) and (6), respectively, generate $H_2$ while the electrochemical oxidation reaction (7), consumes $H_2$ and produces steam at the anode. As the rate of CO oxidation is slower than the rate of $H_2$ oxidation [27–29] and the concentration of CO is lower than the concentration of $H_2$, electrochemical oxidation of CO was not included in the model.

Table 2 summarizes the equations and boundary conditions for the mass transfer calculations. Eq. (8) describes diffusion within the anode structure. All reactions occurring in this system are assumed to take place on the solid surface (i.e., not in the gas phase). The terms on the left-hand side of the equation account for the diffusion in the solid phase while the terms on the right-hand side account for the change in the number of moles of each species through the relevant reactions. The last term accounts for the change in the total number of moles from the steam reforming reaction, Eq. (5), in which the ratio of the moles of products to the moles of reactants is two. The solid structure is assumed to be insulated from all sides and mass transfer is only permitted from the anode to the anode gas channel as shown in the boundary equations in Eq. (9).

Eq. (10) describes convective mass transfer in the anode gas phase. Diffusion of the gases through and from the solid structure is accounted for in this equation and the boundary conditions given in Eq. (11). Diffusion in the direction of flow is neglected and the only boundary condition in that direction is the initial concentration of each species.

Multi-component diffusion coefficients were used for mass transfer in the gas phase, while Knudsen diffusion was used for the diffusion through the porous solid structure of the anode [30]. The effective diffusion coefficient ($D_i^{\text{eff}}$) is a function of the tortuosity of the solid and the gas–solid interactions as given in Eq. (13):

$$\frac{1}{D_i^{\text{eff}}} = \frac{1}{D_i^{\text{Knudsen}}} + \frac{1}{D_{i,\text{gas}}\varepsilon/\tau} \quad (13)$$

Table 2
Equations and boundary conditions used for mass transfer calculations

Within the anode structure

$$\frac{D_i^{\text{eff}}(\partial^2 P_i/\partial x^2 + \partial^2 P_i/\partial y^2 + \partial^2 P_i/\partial z^2)}{RT} = \sum_{j=5,6,7} \text{accordingly}\ \nu_i R_j + \nu_i \frac{i}{2F} + \frac{P_i}{P_i(2R_i)} \quad (8)$$

$$x = 0,\ w_{\text{fc}} \quad y = t_{\text{c}} + t_{\text{e}} \quad y = H_{\text{s}} \quad z = 0,\ L$$
$$\frac{\partial P_i}{\partial x} = 0 \quad \frac{\partial P_i}{\partial y} = 0 \quad D_i^{\text{eff}} \frac{\partial P_i}{\partial y} = -D_{i,\text{g}} \frac{\partial P_i}{\partial y} \quad \frac{\partial P_i}{\partial z} = 0 \quad (9)$$

Gas phase (anode channel)

$$\frac{1}{A_{\text{fc}}} \left( \frac{\partial(\dot{n}_t(P_i/P_t))}{\partial z} \right) - D_{i,\text{g}} \frac{(\partial^2 P_i/\partial x^2 + \partial^2 P_i + \partial y^2)}{RT} = 0 \quad (10)$$

$$\text{At : ab, ef} \quad y = H_{\text{s}} \quad y = H_{\text{fc}}$$
$$\frac{\partial P_i}{\partial x} = 0 \quad D_i^{\text{eff}} \frac{\partial P_i}{\partial y} = -D_{i,\text{g}} \frac{\partial P_i}{\partial y} \quad \frac{\partial P_i}{\partial y} = 0 \quad (11)$$

$$z = 0$$
$$P_{\text{CH}_4} = 0.33 P_{\text{t}} \quad P_{\text{H}_2\text{O}} = 0.67 P_{\text{t}} \quad P_{\text{H}_2} = P_{\text{CO}} = P_{\text{CO}_2} = 0 \quad (12)$$

where $D_i^{\text{Knudsen}}$ is the Knudsen diffusion coefficient for each species $i$, $D_{i,\text{gas}}$ the gas phase diffusion coefficient of species $i$, $\varepsilon$ the porosity, and $\tau$ is the tortuosity.

The steam reforming reaction rate was determined using a simple reaction model of the form shown in Eq. (14) [31]:

$$R_{\text{SR}} = k_0 x_{\text{CH}_4} P_{\text{t}}\, \text{e}^{-E_{\text{act}}/RT_{\text{cb}}} \quad (14)$$

In this equation, the rate of reaction, $R_{\text{SR}}$, depends on the frequency factor, $k_0$, the partial pressure of methane, $x_{\text{CH}_4} \cdot P_{\text{t}}$, activation energy of the reaction, $E_{\text{act}}$, and temperature of the catalyst bed, $T_{\text{cb}}$. The water-gas-shift (WGS) reaction is typically assumed to be at equilibrium throughout the cell [26,32]. In the present work, however, simple kinetic models were used for both forward and backward reactions, as suggested by Lehnert et al. [26].

### 2.2. Heat balances

The unit cell is assumed to be thermally isolated and thus effectively insulated from all sides. Heat is generated or withdrawn from reactions occurring on the surface and within the solid catalyst structure. The reactions considered do not occur in the gas phase at the temperature of interest for this study (i.e., 1073 K). Heat is exchanged between the solid and the gas streams by convection and through transport of reactants and products from or through the solids. Across the solids, heat conduction was considered dominant. The equations and boundary conditions for the heat transfer calculations are given in Table 3.

The electrochemical oxidation consists of two half-cell reactions occurring separately in the anode and cathode, and heat is generated within the electrolyte and the electrodes. The heat generated, however, is assumed to be produced within the anode structure because the cathode and electrolyte are very thin, rel-

Table 3
Equations and boundary conditions used for heat transfer calculations

Within the PEN structure

$$k_{\text{s}} \left( \frac{\partial^2 T_{\text{s}}}{\partial x^2} + \frac{\partial^2 T_{\text{s}}}{\partial y^2} + \frac{\partial^2 T_{\text{s}}}{\partial z^2} \right) = \dot{Q} \quad (15)$$

$$x = 0,\ w_{\text{fc}} \quad z = 0,\ L$$
$$\frac{\partial T}{\partial x} = 0 \quad \frac{\partial T}{\partial x} = 0 \quad (16)$$

$$y = 0 \quad y = H_{\text{s}}$$
$$k_{\text{s}} \frac{\partial T}{\partial y} = h_{\text{air}}(T_{\text{air}} - T_{\text{s}}) + \vec{N}_{\text{O}_2} C_{p,\text{O}_2} T_{\text{air}} \quad -k_{\text{s}} \frac{\partial T_{\text{s}}}{\partial y} = h_{\text{f}}(T_{\text{f}} - T_{\text{s}}) - \sum \vec{N}_i C_{p,i} T_i \quad (17)$$

Within the interconnects structure

$$k_{\text{ic}} \left( \frac{\partial^2 T_{\text{ic}}}{\partial x^2} + \frac{\partial^2 T_{\text{ic}}}{\partial y^2} + \frac{\partial^2 T_{\text{ic}}}{\partial z^2} \right) = 0 \quad (18)$$

$$x = 0,\ w_{\text{fc}} \quad z = 0,\ L \quad \text{At : ab, ef} \quad y = 0,\ H_{\text{s}}\ \text{(solid contacts)} \quad \text{At : ad, eh}$$
$$\frac{\partial T}{\partial x} = 0 \quad \frac{\partial T}{\partial z} = 0 \quad k_{\text{ic}} \frac{\partial T_{\text{ic}}}{\partial x} = h_{\text{air}}(T_{\text{air}} - T_{\text{ic}}) \quad k_{\text{ic}} \frac{\partial T_{\text{ic}}}{\partial y} = -k_{\text{s}} \frac{\partial T_{\text{s}}}{\partial y} \quad k_{\text{ic}} \frac{\partial T_{\text{ic}}}{\partial y} = h_{\text{air}}(T_{\text{air}} - T_{\text{ic}}) \quad (19)$$

Anode and cathode channel

$$h_{\text{air}}[(T_{\text{air}} - T_{\text{s}}) w_{\text{fc}} + (T_{\text{air}} - T_{\text{ic}})(w_{\text{fc}} + H_{\text{fc}})] - w_{\text{fc}} \vec{N}_{\text{O}_2} C_{p,\text{O}_2} T_{\text{air}} = C_{p,\text{air}} \frac{\text{d}\dot{m}_{\text{air}} T_{\text{air}}}{\text{d}z} \quad (20)$$

$$h_{\text{f}}[(T_{\text{f}} - T_{\text{s}}) w_{\text{fc}} + (T_{\text{f}} - T_{\text{ic}})(w_{\text{fc}} + H_{\text{fc}})] + w_{\text{fc}} \sum \vec{N}_i C_{p,i} T_i = C_{p,\text{f}} \frac{\text{d}\dot{m}_{\text{f}} T_{\text{f}}}{\text{d}z} \quad (21)$$

$$z = 0$$
$$T_{\text{air}} = T_{\text{f}} = 1073\ \text{K} \quad (22)$$

ative to the anode. The gases flowing on each side of the PEN structure remove heat from each surface through convection as shown in the boundary conditions in Eqs. (17), (20) and (21). The diffusion of species also contributes to the transfer of heat from the PEN structure to the gas phases. Within the solid structure heat transfer occurred only through conduction as accounted for in Eqs. (15) and (18). The gases enter the channels at 1073 K (Eq. (22)) and all the sides of the solid structure are insulated (Eqs. (16) and (19)).

The rate of heat generation $\dot{Q}$ was determined from

$$\dot{Q} = R_{SR}\Delta H_{SR} + R_{WGS}\Delta H_{WGS} + i\left(\frac{\Delta H_{Ox}}{nF} - V_{cell}\right) \quad (23)$$

where $\dot{Q}$ stands for the rate of heat generation, $\Delta H$ the enthalpy of the steam reforming (SR), water-gas-shift (WGS), or oxidation (Ox) reactions, $i$ the current density at each point, $n$ the number of electrons transferred through the reaction, $F$ the Faraday constant, $V$ the voltage of the cell, and $R$ is the rate of steam reforming or water-gas shift, per surface area of the catalyst.

There is an entrance effect as the gas enters the channels on either side of the PEN structure. In the energy balance analysis, axial variations of the convective heat transfer coefficient, $h$, therefore, are determined and taken into account [33]. The variation in the value of $h$ is larger on the cathode side because the Reynolds number is higher for air.

### 2.3. Electrochemistry

Electrochemical calculations were used to estimate current densities throughout the cell. The reversible cell voltage ($E_{OCV}$) or the "open circuit voltage" (OCV) is a function of temperature and reactant concentrations. The difference between the OCV and the cell operating voltage ($V_{cell}$) equals the sum of ohmic losses (the current density ($i$) times the cell resistance ($R_{ohm}$)), the activation losses or overpotential ($\eta_{act}$), and the concentration overpotentials ($\eta_{conc}$) as follows:

$$E_{OCV} - V_{cell} = R_{ohm}i + \eta_{act} + \eta_{conc} \quad (24)$$

The concentration overpotentials can be relatively large (>0.02 V) when mass transfer is the rate-limiting step of the electrochemical reaction within the cell. For the present case, however, $H_2$ is readily available throughout the anode and the maximum current density is sufficiently low that the concentration overpotential was negligible. This assumption is justified using the results from Aguiar et al. [25] and also by performing calculations at areas having high current densities and low hydrogen concentrations. Thus, for the present model only activation and ohmic losses were considered.

The open circuit voltage, $E_{OCV}$, was evaluated solving the Nernst equation as follows:

$$E_{OCV} = E^0 + \frac{RT}{nF}\ln\left(\frac{P_{H_2}P_{O_2}^{0.5}}{P_{H_2O}}\right) \quad (25)$$

where $E^0$ represents the theoretical potential of the reaction at temperature $T$ and partial pressures $P_{H_2}$, $P_{O_2}$, $P_{H_2O}$ for hydrogen, oxygen and water, respectively, and $R$ is the gas constant.

Table 4
Equations used for calculations of activation overpotentials [1]

$$i_{0,a} = K_a\, e^{-E_{act,a}/RT}\left(\frac{P_{H_2}^{TPB}}{P_t}\right)\left(\frac{P_{H_2O}^{TPB}}{P_t}\right) \quad (26)$$

$$i_{0,c} = K_c\, e^{-E_{act,c}/RT}\left(\frac{P_{O_2}^{TPB}}{P_{O_2}^{ref}}\right)^{1/4} \quad (27)$$

$$i_{cell} = i_{0,electrode}\left[\exp\left(\frac{\alpha n_e F}{RT\eta_{act,electreode}}\right) - \exp\left(\frac{(1-\alpha)n_e F}{RT\eta_{act,electrode}}\right)\right] \quad (28)$$

The equations used for exchange current densities and overpotential calculations are listed in Table 4. For activation overpotential calculations, the Butler–Volmer equation was applied separately to the anode and the cathode. The values of the activation overpotential depend on the nature of the reaction, the catalyst and the temperature. These dependences are included in the values of exchange current densities, $i_0$. The data used for the overpotential calculations were obtained from the work of Costamagna and co-workers [1,34].

## 3. Results and discussion

In this section, the model results for the concentration and current density profiles along the length of the cell will be discussed first. The results for the methane to steam ratio will then be presented and the susceptibility of different areas of the cell to deposition of carbon based on this ratio will be examined. The temperature distributions along the length and through the cross-section of the unit cell will be given and the resulting temperature gradients shown. Finally the effects of recycling of the anode exhaust gas on both the temperature distribution and the methane to steam ratio will be discussed.

### 3.1. Concentration and current density profile

Average gas phase concentrations of reactants and products along the length of the cell are shown in Fig. 2. The rapid depletion of $CH_4$ and $H_2O$ and the corresponding increase in

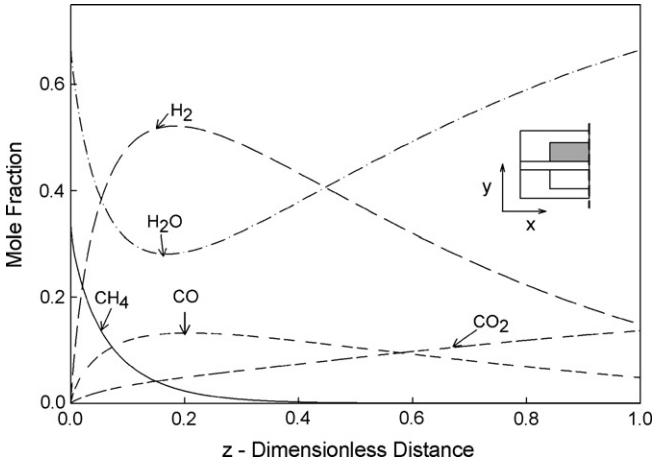


Fig. 2. Bulk-mean anode gas phase composition along the length of the cell. In this and all following figures, the relevant section of the unit cell is indicated in the inset.

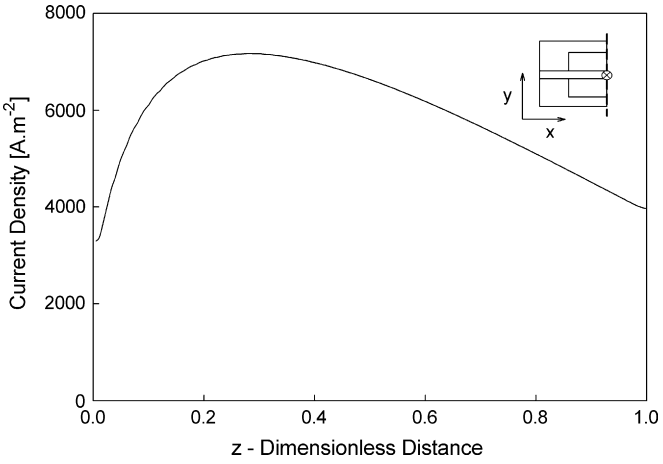


Fig. 3. Current density in the mid-plane of the PEN structure along the length of the cell.

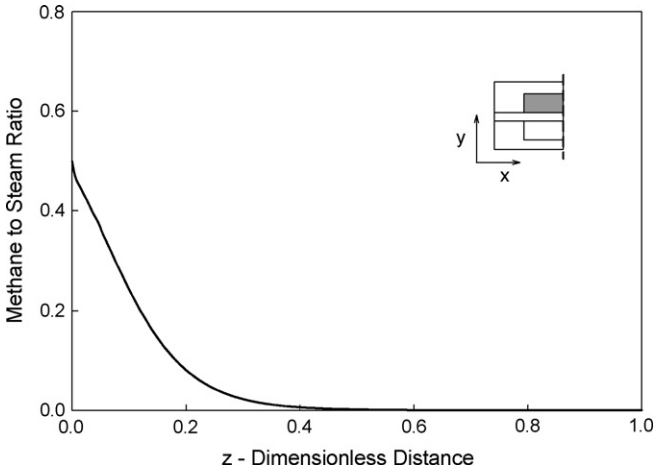


Fig. 4. Ratio of methane to steam in the gas phase along the length of the cell.

$H_2$ concentration indicates that steam reforming occurs mainly at the entrance to the cell ($z<0.2$). The produced $H_2$ is then consumed by the electrochemical reaction such that the $H_2$ concentration reaches a maximum at approximately 20% along the length of the cell ($z=0.2$). Correspondingly, there is a minimum in the $H_2O$ concentration because $H_2O$ is consumed by the reforming reaction and produced by the $H_2$ oxidation reaction. The distributions of CO and $CO_2$ along the length of the cell are in agreement with equilibrium calculations for $z>0.2$. At the inlet region ($z<0.1$), however, CO is produced so quickly by steam reforming that the water-gas shift reaction does not reach equilibrium. These trends in concentration are in agreement with the calculations of Aguiar et al. [25].

The current densities, calculated in the mid-plane of the PEN structure, are shown in Fig. 3. The current density increases to a maximum at $z\approx0.25$. The maximum in the current density does not occur at the same location as the maximum in the $H_2$ concentration because the current density depends on the temperature as well as the concentration of $H_2$ (see equations in Table 4). That is, the temperature of the anode changes along the length of the cell as the relative rates of the exothermic and endothermic reactions change. The temperature profile will be discussed in Section 3.3.

### 3.2. Methane to steam ratio

In terms of carbon deposition, the main parameters of interest are the concentration of methane and the steam to hydrocarbon ratio. The steam to hydrocarbon ratio increases along the length of the cell as the steam and methane react to form hydrogen, which then electrochemically reacts to form steam (Fig. 2). In Fig. 4, the data are presented in terms of the methane to steam ratio, which varies between 0 and 0.5 (the steam to methane ratio varies between infinity and 2). At the inlet of the cell, the ratio of methane to steam is 0.5, and this ratio decreases throughout the length of the cell as methane is consumed and steam is produced. Thus, the inlet of the cell is the most susceptible area for carbon formation.

The cross-sectional distribution of the methane to steam ratio within the anode at the inlet ($z=0.005$) is illustrated in the contour plot in Fig. 5. The letters (a, d, e, and h) correspond to the same letters used in Fig. 1b. The rate of change in the methane to steam ratio with distance into the anode indicates that the majority of the steam reforming reaction occurs in the top portion of the anode, closest to the fuel channel and furthest from the triple-phase boundary, at which the fuel, oxygen anions and catalyst meet. The methane to steam ratio continuously decreases from the gas/anode interface (line ad) through the anode structure to the anode/electrolyte interface (close to line eh—the electrolyte and cathode are very thin relative to the anode). According to the methane to steam ratio, the area that is most susceptible to carbon formation is the catalyst at the gas/anode interface at which the steam to carbon ratio is lowest, and to which the oxygen anions will not penetrate.

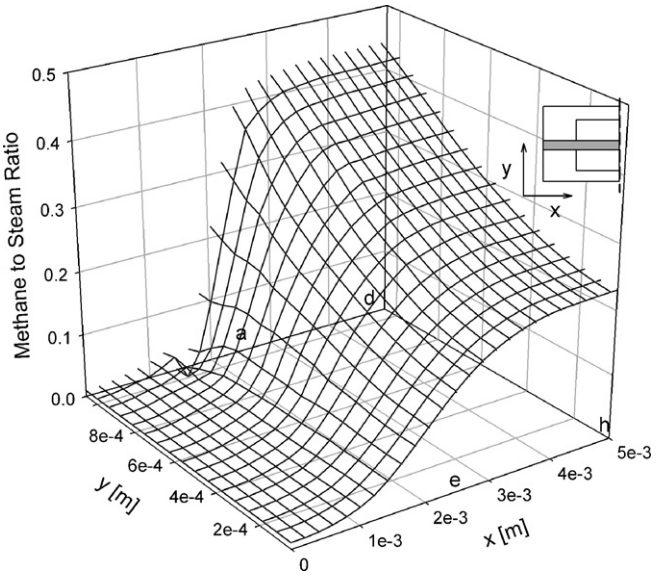


Fig. 5. Contour plot of methane to steam ratio in the *XY* plane of the anode at $z=0.005$. Note that the values for $x$ and $y$ are the actual distances. The concentration of methane is essentially zero under the interconnect.

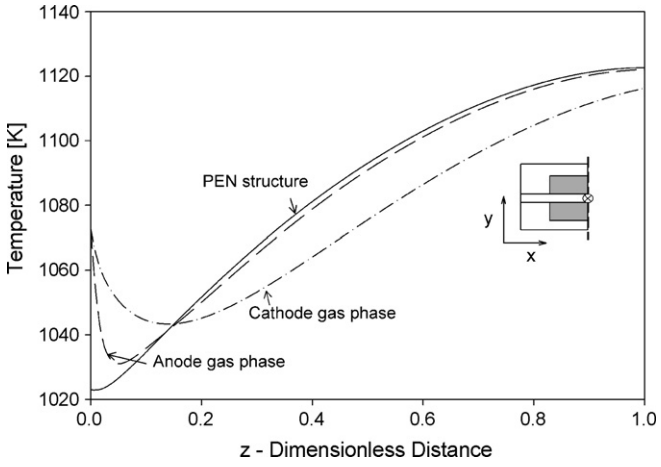


Fig. 6. Bulk-mean temperature in the gas phases along the length of the cell and temperature along the mid-plane of the PEN structure. Because the PEN structure is thin, temperature variation in the *y*-direction is negligible.

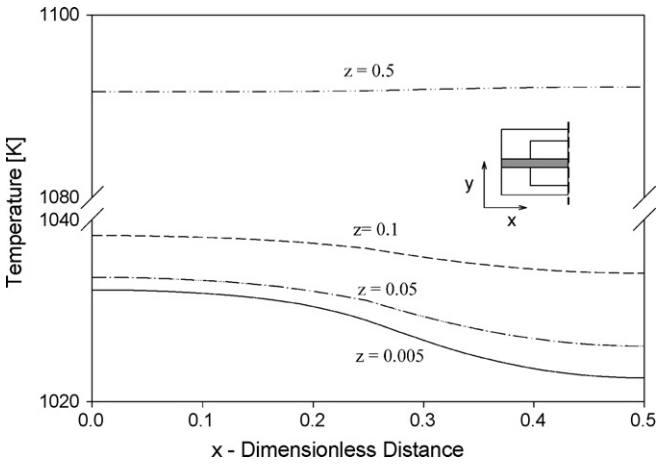


Fig. 7. Temperatures in the PEN structure vs. position in the direction lateral to that of flow. *Z* represents the dimensionless distance from the gas inlet, along the flow direction. Temperature variations in the *y*-direction are negligible.

### 3.3. Temperature distribution

In this section, temperature distributions in three dimensions for each of the gas and solid phases are discussed. Calculated bulk-mean gas phase temperature distributions are shown in Fig. 6. Also included is the temperature profile in the flow direction at the mid-plane of the solid phase (PEN structure). The temperature of the solid phase is lowest at the inlet where the rate of the endothermic steam reforming reaction is the highest. The solid phase is approximately 50 K cooler than the temperature of the inlet gases. As the exothermic electrochemical oxidation reaction rate increases, the temperature increases along the length of the cell. The temperature of the gas-phase on the anode side is close to the temperature of the solid phase. There is a lag in the temperature at the gas inlet while the gas cools to the temperature of the solid. On the cathode side, the gas flow rate is substantially higher than that on the anode side. Changes in the air temperature are therefore less dramatic than that for the anode gas phase. Temperature gradients in the PEN structure, along the length of the cell, are relatively large and attain a maximum value of 16.4 K cm$^{-1}$ at $z \approx 0.25$.

A balance on the total heat required, taking into account both the endothermic reforming reactions and the exothermic electrochemical and WGS reactions, indicates that even if the total amount of cooling could be distributed evenly throughout the cell, the outlet temperature would be approximately 1120 K. That is, a net excess of heat is generated. The maximum temperature gradient, however, would decrease to ~7–9 K cm$^{-1}$ as the minimum temperature would be 1073 K, the inlet temperature of the gases, compared to 1023 K in the current configuration.

Both the longitudinal (*z*-axis) distribution of temperature and the cross-sectional profiles (*x*–*y* plane) of temperature determine thermal stresses in the materials. Calculations show that the maximum temperature difference across the PEN structure (in the *y*-direction) is within 1 K. Therefore, gradients in the *y*-direction are small, as would be expected for a solid with high thermal conductivity and with a relatively thin PEN structure. Heat is also well dissipated through the interconnects.

Along the length of the cell, however, the distribution of temperature within the PEN structure in the *x*-direction varies considerably. To illustrate the gradients in the *x*-direction, the temperature distributions of four planes from $z = 0.005$ (inlet of cell) to $z = 0.5$ (midway along length of cell) are plotted in Fig. 7. At the inlet, the temperature difference between the PEN structure under the interconnect and the PEN structure at the middle of the cross-section is 10 K with a maximum temperature gradient of 35 K cm$^{-1}$. Mid-way along the length of the cell, however, this temperature difference is less than 1 K and the temperature gradient is negligible. The temperature gradients in the *x*-direction are a result of the fact that only part of the PEN structure is in contact with the interconnect, which effectively dissipates heat. Note that the maximum values of the temperature gradients in the *x*-direction are significantly larger than those in the *z*-direction along the pathway of the gases (i.e., 35 K cm$^{-1}$ versus 16 K cm$^{-1}$). This fact illustrates the significance and importance of 3D modeling in systems that include internal reforming.

These calculations were performed using a co-current flow of gases. Running the model using a counter-current flow pattern resulted in significantly higher temperature gradients, especially at the inlet region of the cell. The maximum value of the gradients in the counter-current configuration was more than 40% higher than in a co-current flow system. These results are in agreement with those reported by Aguiar et al. [25] for planar systems and by Li and Chyu [35] for tubular systems.

### 3.4. Applicability of results to stack analysis

For the heat balance calculations all the cell outer surfaces were assumed to be insulated. This assumption is applicable to the case of a single stand alone cell. For cells in a stack, however, the heat transfer from one cell to another also should be taken into account, as the top surface of each cell is in contact with the bottom surface of the next cell. The calculated temperatures on the top and bottom surfaces of the cell along the pathway are plotted in Fig. 8. As shown, these values are within 5 K (and

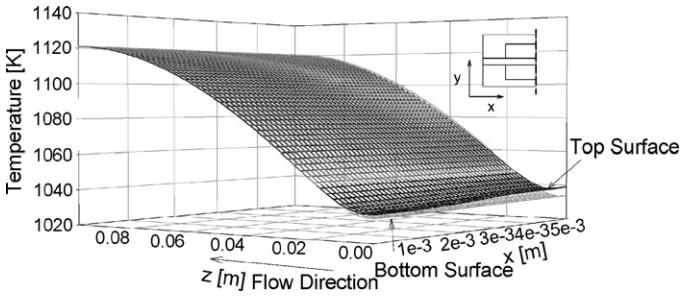


Fig. 8. Temperature of the top and bottom surfaces of the interconnect plates along the length of the cell.

actually within 1 K for over 90% of the cell) throughout the cell, such that there will be little if any heat transfer between cells in a stack, and the distribution of temperature within the PEN structure calculated in this study is applicable to either a single cell or a cell within a stack. To further verify this result, a "two-adjacent-cell" system was modeled. Although the temperature distribution in the interconnects changed slightly, the temperature distribution in the PEN structure for the two-adjacent-cell system was identical to the distribution obtained for the single cell system.

### 3.5. Recycling

The effects of recycling on the temperature distribution for 50, 60 and 75% recycling of the anode exhaust gas are shown in Fig. 9. The percent of recycling is defined as the amount of recycled gas divided by the total amount of anode outlet gas multiplied by 100%. As mentioned in Section 1, recycling results in a dilution of the methane concentration and enrichment in the hydrogen concentration in the feed. The higher hydrogen concentration in the feed results in a higher current density at the inlet region with a corresponding increase in the temperature. The higher the fraction of recycling the smaller the temperature difference between the inlet ($z=0$) and outlet ($z=1$) of the unit cell (Fig. 9a). The maximum temperature gradient decreased from 16 K cm$^{-1}$ for no recycling to almost 10 K cm$^{-1}$ for a recycling ratio of 75%.

Recycling also influences the cross-sectional temperature distribution of the PEN structure (Fig. 9b). Note that the temperature difference is plotted in the $y$-axis of Fig. 9b for ease of comparison. The absolute temperature of the PEN structure will be different for each level of recycling. Consistent with the result in the $z$-direction, increasing the amount of recycling decreases the temperature difference in the $x$-direction within the PEN structure. The temperature gradients at the inlet region ($z=0.005$) decreased from 35 K cm$^{-1}$ with no recycling to 11 K cm$^{-1}$ with 75% recycling.

The steam concentration within the cell is also a function of the amount of recycling. With a higher concentration of hydrogen in the feed, the rate of the electrochemical reaction increases and more steam is produced. The calculated inlet concentrations and average current densities for various levels of recycling are listed in Table 5. With 50 and 60% recycling, the steam to methane ratio at the inlet was the same as that with no recycling. For 75% recycling, the steam to methane ratio increased. Although an increase in steam concentration is advantageous in terms of reducing carbon formation, the relative amount of hydrogen decreases as the amount of steam increases, with a resulting decrease in the average current density of the system. Thus, an intermediate level of recycling may be optimal depending on the system parameters.

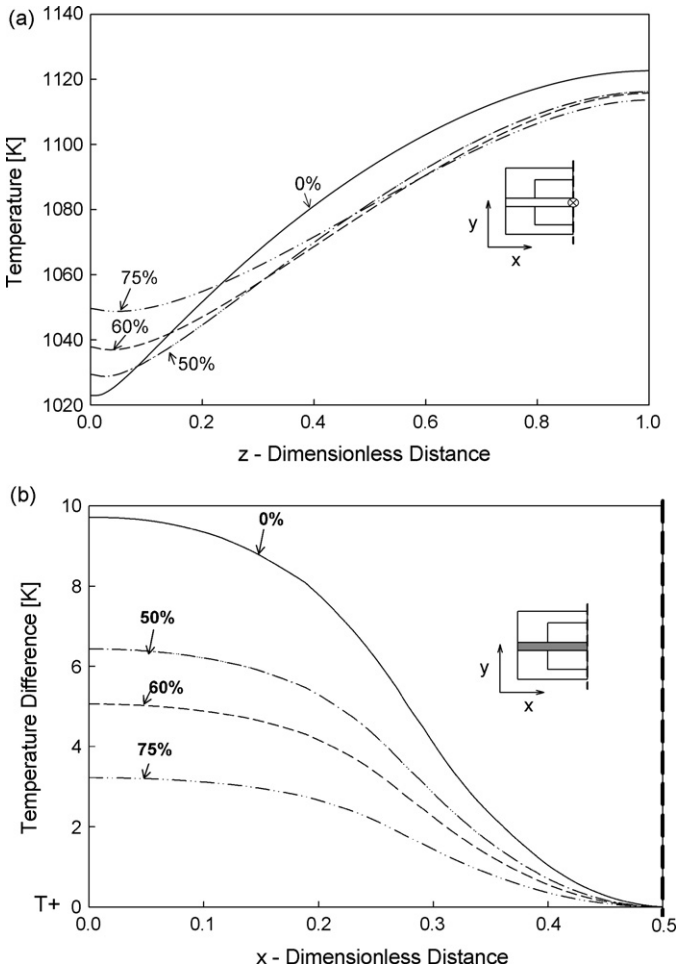


Fig. 9. Temperature distribution of the PEN structure for different levels of recycling: (a) along the length of the cell and (b) through the cross-section at $z=0.005$. The temperature variation in the $y$-direction is negligible.

The susceptibility to carbon formation will be influenced by recycling the anode exhaust gases in several ways. First, the hydrogen to hydrocarbon ratio is higher in the feed. Second, the increased hydrogen content will result in a higher amount

Table 5
Inlet concentration and average current density as a function of recycling level

| Level of recycling (%) | Inlet concentration (mol%) | | | | | Average current density (A cm$^{-2}$) |
|---|---|---|---|---|---|---|
| | $CH_4$ | $H_2O$ | $H_2$ | CO | $CO_2$ | |
| 0 | 33.0 | 67.0 | 0 | 0 | 0 | 0.62 |
| 50 | 21.7 | 43.5 | 13.0 | 8.5 | 13.3 | 0.66 |
| 60 | 16.5 | 34.4 | 24.6 | 11.0 | 13.5 | 0.71 |
| 75 | 10 | 42 | 18 | 12.5 | 17.5 | 0.55 |

of steam at the triple-phase boundary. Third, the increase in the concentration of $CO_2$ in the feed will increase the rate of carbon removal through reaction (4). Offsetting these effects, however, is the increase in the amount of CO with increasing levels of recycling. The WGS reaction is equilibrium limited at 1073 K and, thus, the ratio of CO to $CO_2$ increases as the level of recycling increases. The increasing amount of CO will impede removal of carbon from the surface by shifting the equilibrium of reaction (2).

## 4. Conclusions

A 3D model has been developed to investigate the thermal and electrochemical behavior of an anode-supported SOFC operating nominally at 1073 K with direct internal reforming of methane. The model was developed for a single cell but is applicable to the analysis of a stack because of the minimal (<5 K) temperature difference between the top and bottom of the interconnect structures. The results of the developed model indicate that significant temperature gradients exist both along the length of the cell (up to $16\,K\,cm^{-1}$) and within the cross-section of the cell (up to $35\,K\,cm^{-1}$), specifically at the inlet to the cell. The identification of the temperature gradients within the cross-section of the cell is only possible with the use of a 3D model. The 2D models previously presented in the literature are deficient in this respect. The relatively large temperature gradients are a result of the relative rates of the endothermic methane steam reforming reaction and exothermic electrochemical reaction at different locations in the PEN structure. These large temperature gradients can be reduced by recycling a percentage of the anode exhaust gases, which changes the composition of the feed. The increased concentration of $H_2$ increases the (exothermic) electrochemical reaction, thus reducing the temperature decrease at the inlet of the cell, while the increased concentrations of $H_2$, $H_2O$ and $CO_2$ may also decrease the amount of carbon deposition. There is an optimal level of recycling, however, in terms of minimizing the temperature gradients and carbon formation, and maximizing the average current density.

## Acknowledgements

The authors acknowledge funding support from the Alberta Energy Research Institute and Western Economic Diversification for this project.

## References

[1] P. Costamagna, A. Selimovic, M. Del Borghi, G. Agnew, Chem. Eng. J. 102 (2004) 61.
[2] M. Boder, R. Dittmeyer, J. Power Sources 155 (2006) 13–22.
[3] K. Ahmed, K. Foger, Catal. Today 63 (2000) 479–487.
[4] P. Heidebrecht, K.S. Sundmacher, J. Power Sources 145 (2005) 40–49.
[5] R. Fellows, J. Power Sources 71 (1998) 281–287.
[6] H. He, J.M. Hill, Appl. Catal. A: Gen. 317 (2007) 284.
[7] H.S. Bengaard, J.K. Norskov, J. Sehested, B.S. Clausen, L.P. Nielsen, A.M. Molenbroek, J.R. Rostrup-Nielsen, J. Catal. 209 (2002) 365–384.
[8] C.M. Finnerty, N.J. Coe, R.H. Cunningham, R.M. Ormerod, Catal. Today 46 (1998) 137–145.
[9] Y.B. Lin, Z.L. Zhan, J. Liu, S.A. Barnett, Solid State Ionics 176 (2005) 1827–1835.
[10] K.M. Walters, A.M. Dean, H.Y. Zhu, R.J. Kee, J. Power Sources 123 (2003) 182–189.
[11] S.L. Douvartzides, F.A. Coutelieris, A.K. Demin, P.E. Tsiakaras, AIChE J. 49 (2003) 248–257.
[12] K. Eguchi, H. Kojo, T. Takeguchi, R. Kikuchi, K. Sasaki, Solid State Ionics 152/153 (2002) 411.
[13] S. Park, R. Craciun, J.M. Vohs, R.J. Gorte, J. Electrochem. Soc. 146 (1999) 3603–3605.
[14] J.H. Koh, B.S. Kang, H.C. Lim, Y.S. Yoo, Electrochem. Solid State Lett. 4 (2001) A12.
[15] C.H. Bartholomew, Catal. Rev. Sci. Eng. 24 (1982) 67–112.
[16] A. Abudula, M. Ihara, H. Komiyama, K. Yamada, Solid State Ionics 86-8 (1996) 1203–1209.
[17] T. Iida, M. Kawano, T. Matsui, R. Kikuchi, K. Eguchi, J. Electrochem. Soc. 154 (2007) B234.
[18] J. Kapicka, N.I. Jaeger, G. Schulz-Ekloff, Appl. Catal. A: Gen. 84 (1992) 47.
[19] R. Peters, R. Dahl, U. Kluttgen, C. Palm, D. Stolten, J. Power Sources 106 (2002) 238–244.
[20] V. Hacker, G. Faleschini, H. Fuchs, R. Fankhauser, G. Simader, M. Ghaemi, B. Spreitz, K. Friedrich, J. Power Sources 71 (1998) 226.
[21] S.H. Clarke, A.L. Dicks, K. Pointon, T.A. Smith, A. Swann, Catal. Today 38 (1997) 411.
[22] E.P. Murray, T. Tsai, S.A. Barnett, Nature 400 (1999) 649.
[23] T. Osaki, T. Mori, React. Kinet. Catal. Lett. 89 (2006) 333–339.
[24] L. Petruzzi, S. Cocchi, F. Fineschi, J. Power Sources 118 (2003) 96.
[25] P. Aguiar, C.S. Adjiman, N.P. Brandon, J. Power Sources 138 (2004) 120–136.
[26] W. Lehnert, J. Meusinger, F. Thom, J. Power Sources 87 (2000) 57–63.
[27] M.A. Khaleel, Z. Lin, P. Singh, W. Surdoval, D. Collin, J. Power Sources 130 (2004) 136.
[28] M. Cimenti, J.M. Hill, Proceedings of the 10th International Symposium on SOFCs, Nara, Japan, 2007.
[29] P. Holtappels, L.G.J.D. Haart, U. Stimming, I.C. Vinke, M. Mogensen, J. Appl. Electrochem. 29 (1999) 561.
[30] Institut für Werkstoffe der Elektrotechnik (IWE), The Numerical Simulation of Fuel Cells of the PEMFC and SOFC type with the Finite Difference Element Method (FDEM). A report on: www.iwe.uni-karlsruhe.de, 2005.
[31] E. Achenbach, E. Riensche, J. Power Sources 52 (1994) 283.
[32] J.M. Moe, Chem. Eng. Progr. 58 (1962) 33.
[33] W. Kays, M. Crawford, B. Wiegand, Convective Heat and Mass Transfer, McGraw-Hill, 2005.
[34] P. Costamagna, K. Honegger, J. Electrochem. Soc. 145 (1998) 3995.
[35] P.W. Li, M.K. Chyu, J. Power Sources 124 (2003) 487.